

# Prebending effects upon the vibrational modes of thermally prestressed planar beams

Fabien Treyssède\*

*Laboratoire Central des Ponts et Chaussées, Division Métrologie et Instrumentation, Route de Pornic, BP 4129,  
44341 Bouguenais Cedex, France*

Received 11 August 2006; received in revised form 5 July 2007; accepted 5 July 2007

---

## Abstract

In this paper, the linear vibrations of thermally prestressed beams are studied including the effects of predisplacement due to prebending and initial imperfections. Only low prestressed states far from the buckling stage are considered, one of the motivations of this paper being the issue of taking into account climatic temperature effects in damage detection based on modal techniques. A brief general review is first presented in order to give some theoretical and physical insights upon structural vibrations superimposed on an initial static state. Both the total Lagrangian and the updated Lagrangian formulations are applied to a planar Euler–Bernouli beam under the assumption of small prestrains and large predisplacements. The governing equilibrium equations are solved using a finite element method. Some illustrative numerical results are given. The model is then validated through experiments inside a climatic chamber. It is concluded that in addition to the axial prestress, the presence of prebending is also likely to have a significant effect upon some eigenfrequencies, even in the case of rather small predisplacements.

© 2007 Elsevier Ltd. All rights reserved.

---

## 1. Introduction

For thin structures such as beams, plates, or shells, the effects of prestress are enhanced by the slenderness ratio. They are thus likely to have a significant impact upon dynamics, even for relatively low prestressed states far from the buckling stage. In the context of linear dynamics, the presence of prestress acts upon modal parameters, with a stronger shifting effect for lower eigenfrequencies in practice.

As far as beams are concerned, the natural frequencies of flexural vibration increase (resp. decrease) when the axial load is tensile (resp. compressive). The eigenfrequencies of Euler–Bernouli axially prestressed beams have been analytically studied with various boundary conditions [1]. Some experimental/numerical comparisons have also been done including nonlinear effects [2]. Mead [3] has used a semi-analytical method to analyze some self-strained planar frames. Law et al. [4] have numerically shown some effects of axial prestressing upon time responses. Some other studies focused upon prestressed concrete bridges [5,6]. Timoshenko beams, including transverse shear strains, have also been analyzed with analytical methods [7–9]. Yokoyama [10] compared the experimental eigenfrequencies of self-weighted beams (under gravity) with those

---

\*Tel.: +33240845932; fax: +33240845998.

E-mail address: [fabien.treysede@lcpc.fr](mailto:fabien.treysede@lcpc.fr)

obtained from a finite-element model. Naguleswaran [11] considered beams subject to linearly varying axial force. Ganesan et al. [12] used a finite element (FE) method to analyze the in-plane prestressed vibration as well as the linear buckling of sandwiches beams under thermal environments with temperature-dependent material properties.

Axially prestressed beams have obviously received much attention in the literature, and the references cited above are far from being exhaustive. Nevertheless, the effects of predisplacement, which may be due to prebending or initial imperfections, are hardly considered although some early works have analytically and experimentally demonstrated its potential effect upon vibration [13–17].

As far as static stability is concerned, the non-negligible effect of initial displacement is rather well-known in nonlinear buckling analysis and has been the subject of much research. More scarcely, some authors extended their analyses to the effect upon dynamics. For instance, Perkins [18] investigated the linear vibrations of a simply supported arch with initial curvature effects for a wide range of post-buckling loads. The author used a Galerkin method and made a comparison with experimental measurements. Nayfeh et al. [19] analytically and experimentally studied the natural frequencies and mode shapes of buckled beams (with the first buckling mode) for hinged and clamped boundary conditions. Chen et al. [20] employed a Galerkin method to study the vibration and buckling of circular arches under uniform initial bending stress, but its influence remained obscure. For the design of microelectromechanical systems, Paul et al. [21] made an analytical and experimental study of buckling and vibration of thin film sandwiches taking into account static predeflection. Teng et al. [22] chose a numerical shooting method to analyze the vibration of thermally post-buckled beams. Addressi et al. [23] proposed a Galerkin method to investigate the sensitivity of the modal properties in the vicinity of the first buckling Euler load.

In fact to the author's knowledge, results available in the literature including predisplacement effects on structural dynamics are generally focused on post-buckling configurations, for which some static deflection always exists even for straight beams. Surprisingly, prebending effects upon vibrations are hardly outlined for low non-buckled prestressed states (and often neglected), particularly for thermally prestressed beams. Based on a general FE procedure, the goal of this paper is to highlight the influence of predisplacement upon the modal parameters of planar beams subject to moderate thermal prestress.

This study is motivated by the need of adequate numerical models for thermally prestressed dynamics, which is of great importance within the framework of robust vibration control [24–26] or efficient structural health monitoring based on modal diagnosis [27–29] with thermal compensation. Typical applications in civil engineering are a bridge or a building subjected to climatic thermal variations [30–32] (for such structures, the daily variation of natural frequency may reach several percent).

In this paper, a brief theoretical review is first given in order to clarify the general equilibrium equations of structural vibrations superimposed on an arbitrary initial static state. In order to simply illustrate the influence of prebending, the theory is applied to planar beams subjected to prestressed states of small strain and large displacement. The equilibrium equations, which take into account the presence of predeformation in addition to the classical axial prestress, are solved using a FE method. A brief numerical example is studied in order to highlight some prebending effects induced by a thermal gradient through the thickness. Finally, a laboratory test-case is driven inside a climatic chamber. Experimental and FE results are compared. Initial imperfections, inevitably occurring in real-life structures, are included in the whole analysis.

## 2. General equations

In prestressed dynamics, three configurations must be distinguished: the reference configuration (undeformed and unprestressed), the predeformed configuration (corresponding to the prestressed state), and the total configuration (including superimposed dynamical deformations). Quantities referring to these configurations will, respectively, be denoted with a subscript “ref”, a subscript 0 and a tilde. The absence of symbol will be left for superimposed dynamical quantities. In this paper, the reference configuration represents the ideal geometry without initial imperfections, which are denoted by the subscript  $i$ . Fig. 1 illustrates these geometrical configurations for a vibrating straight ideal beam subjected to prebending.

We restrict our study to conservative systems, linear thermoelastic constitutive laws, static (or quasi-static) prestressed states, and small superimposed vibrations. The prestress/predeformation effects are viewed by

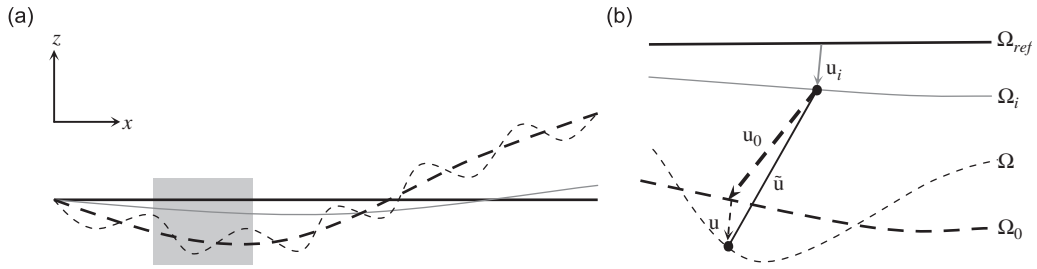


Fig. 1. (a) Reference  $\Omega_{ref}$  (straight bold line), predeformed  $\Omega_0$  (bold dashed), total  $\Omega$  (dashed) and imperfect  $\Omega_i$  (thin line) configurations for an idealized straight beam. (b) Zoom of the gray zone with the particle displacement decomposition.

dynamics through the geometric nonlinearities of the prestressed state, possibly in large prestrain. Furthermore, the hypothesis of a weak coupling between temperature and mechanical deformation is made, in the sense that mechanically induced heating is neglected. The period of vibrational displacements is supposed to be far smaller than temperature fluctuations in time, meaning that thermally induced vibrations are not considered:  $\tilde{T} \equiv T_0$  (temperature acts upon dynamics only through the prestressed state).

This section briefly reviews the formulations of governing equilibrium equations. Further theoretical details, for instance, will be found in Refs. [33–35].

### 2.1. Total configuration equilibrium

The mechanical model requires at the beginning of the analysis the consideration of the large deformations of the system. Based on a Lagrangian formulation, Hamilton’s principle for the total configuration writes

$$\delta \int_{t_1}^{t_2} (\tilde{T} - \tilde{V} - \tilde{V}_{ext}) dt = 0 \quad \text{with} \quad \delta \tilde{\mathbf{u}}(t_1) = \delta \tilde{\mathbf{u}}(t_2) = 0 \quad \text{and} \quad \tilde{\mathbf{u}}|_{\Gamma_{ref}^u} = \tilde{\mathbf{u}}, \quad (1)$$

where  $\tilde{T}$  is the total kinetic energy,  $\tilde{V}$  the total strain energy and  $\tilde{V}_{ext}$  the external energy, given by

$$\tilde{T} = \frac{1}{2} \int_{\Omega_{ref}} \rho_{ref} \dot{\tilde{\mathbf{u}}} \cdot \dot{\tilde{\mathbf{u}}} d\Omega; \quad \tilde{V} = \frac{1}{2} \int_{\Omega_{ref}} \tilde{\mathbf{E}} : \tilde{\mathbf{S}} d\Omega; \quad \tilde{V}_{ext} = - \int_{\Omega_{ref}} \rho_{ref} \tilde{\mathbf{u}} \cdot \tilde{\mathbf{f}} d\Omega - \int_{\Gamma_{ref}^T} \tilde{\mathbf{u}} \cdot \tilde{\mathbf{T}} d\Gamma. \quad (2)$$

$\Omega_{ref}$  corresponds to the geometry of the ideal and undeformed structure.  $\Gamma_{ref}^u$  and  $\Gamma_{ref}^T$  are its associated boundaries ( $\partial\Omega_{ref} = \Gamma_{ref}^T \cup \Gamma_{ref}^u$ ) and, respectively, denote surfaces associated with essential (prescribed displacement) and natural (prescribed stress) boundary conditions. Within the scope of linear thermoelasticity, the stress–strain relationships are  $\tilde{\mathbf{S}} = \mathbf{\Lambda} : \tilde{\mathbf{E}} - \mathbf{\kappa}\theta_0$ .  $\tilde{\mathbf{u}}$  is the total displacement.  $\tilde{\mathbf{E}}$  and  $\tilde{\mathbf{S}}$  are, respectively, the total nonlinear Green–Lagrange strain tensor and the second Piola–Kirchhoff stress tensor.  $\theta_0$  is equal to  $T_0 - T_{ref}$ , the temperature difference with respect to the reference temperature (i.e. for which there is no thermal stresses).  $\tilde{\mathbf{f}}$  is the total external body force per unit mass.  $\rho_{ref}$  denotes the reference material density  $\mathbf{\Lambda}$  and  $\mathbf{\kappa}$ , respectively, denote the tensors of elasticity and thermal material properties. In the presence of initial imperfections  $\mathbf{u}_i$  (which are supposed to be known), the Green–Lagrange strain tensor must include some additional terms (see for instance Ref. [36] or [37]):

$$\tilde{\mathbf{E}} = \frac{1}{2} (\nabla \tilde{\mathbf{u}} + \nabla \tilde{\mathbf{u}}^T + \nabla \tilde{\mathbf{u}}^T \nabla \tilde{\mathbf{u}} + \nabla \mathbf{u}_i^T \nabla \tilde{\mathbf{u}} + \nabla \tilde{\mathbf{u}}^T \nabla \mathbf{u}_i). \quad (3)$$

This expression derives from the fact that initial imperfections are defined as static deformations without stress or strain ( $\mathbf{S}_i = \mathbf{E}_i = 0$ ).

Because a Lagrangian formulation has been used, it should be outlined that all quantities and derivatives in the above equations are written in terms of material coordinates in the reference configuration.

### 2.2. Linearized total and updated Lagrangian formulations

Now, the total displacement vector is decomposed as a sum of two components, one corresponding to the prestressed state, and the other corresponding to small superimposed non-stationary perturbations

Table 1  
Definitions of notations involved in Eq. (4)

Formulation	$\Omega, \Gamma^{u,T}, \nabla$	$\mathbf{e}$ (incremental strain)	$\boldsymbol{\sigma}$ (inc. stress)	$\rho$	$\boldsymbol{\sigma}_0$
Total	$\Omega_{\text{ref}}, \Gamma_{\text{ref}}^{u,T}, \nabla_{\text{ref}}$	$\frac{1}{2}(\nabla \mathbf{u} + \nabla \mathbf{u}^T + (\nabla \mathbf{u}_0 + \nabla \mathbf{u}_i)^T \nabla \mathbf{u} + \nabla \mathbf{u}^T (\nabla \mathbf{u}_0 + \nabla \mathbf{u}_i))$	$\mathbf{A}:\mathbf{e}$	$\rho_{\text{ref}}$	2nd Piola–Kirchhoff
Updated	$\Omega_0, \Gamma_0^{u,T}, \nabla_0$	$\frac{1}{2}(\nabla \mathbf{u} + \nabla \mathbf{u}^T)$	$\mathbf{C}:\mathbf{e}$	$\rho_0$	Cauchy stress

(see Fig. 1):  $\tilde{\mathbf{u}} = \mathbf{u}_0 + \mathbf{u}$ . The prestressed state variables are assumed to verify Hamilton's principle (1) for the static case. Keeping only quadratic terms in  $\mathbf{u}$  (for the purpose of linearization), the following Hamilton's principle holds for the superimposed dynamic state with the following energy expressions:

$$\begin{aligned}
 T &= \frac{1}{2} \int_{\Omega} \rho \dot{\mathbf{u}} \cdot \dot{\mathbf{u}} \, d\Omega; & V &= \frac{1}{2} \int_{\Omega} \mathbf{e} : \boldsymbol{\sigma} \, d\Omega + \frac{1}{2} \int_{\Omega} \text{tr}(\nabla \mathbf{u} \boldsymbol{\sigma}_0 \nabla \mathbf{u}^T) \, d\Omega, \\
 V_{\text{ext}} &= - \int_{\Omega} \rho \mathbf{u} \cdot \mathbf{f} \, d\Omega - \int_{\Gamma^T} \mathbf{u} \cdot \bar{\mathbf{T}} \, d\Gamma.
 \end{aligned} \tag{4}$$

The definitions of notations involved in the above expressions are summarized in Table 1 and depend on the choice of the formulation, namely the linearized total Lagrangian formulation or the linearized updated Lagrangian formulation (for further details, see for example Refs. [33,34]). The former is obtained from a direct linearization of the formulation exposed in Section 2.1. The latter can be obtained by applying a transformation from Lagrange to Euler variables. The second term in the expression of  $V$  is the so-called geometric stiffness energy. For thin structures, it corresponds to the effect of in-plane prestress (axial prestress for beams).

What should be understood with the updated Lagrangian formulation is that every quantity ( $\mathbf{u}$ ,  $\mathbf{f}$ , the operator  $\nabla(\cdot), \dots$ ) is written in terms of the Eulerian coordinates in the predeformed configuration.  $\Omega_0$  corresponds to the geometry of the prestressed structure (i.e. in its predeformed configuration, including initial imperfections). In the context of FE methods, this means that the meshing should be done over the predeformed geometry. It should also be noted that the coefficients of the constitutive tensors  $\mathbf{A}$  and  $\mathbf{C}$  used in the total and updated Lagrangian formulations are rigorously not identical. To be more precise, as shown in Ref. [33], using the same coefficients for both incremental laws can lead to significant differences in the case of large strain. However, under the conditions of small strain—which will be the hypothesis adopted in the remaining of this paper—the use of identical material coefficients yields practically the same results for both formulations.

### 3. Application to planar beams

In this section, the equations governing the dynamic equilibrium of a planar Euler–Bernouli beam are derived from a total Lagrangian formulation. Based on a Von Karman approximation, small prestrain, moderate prerotation and large predisplacement are assumed. This kind of model is one of the simplest geometrically nonlinear models but its degree of nonlinearity will be high enough given our interest in moderate prestress states in this paper. A FE method is chosen to solve the equations. The updated Lagrangian formulation is also considered by approximating the predeformed geometry as a composition of straight beam segments.

#### 3.1. Basic assumptions and total configuration equilibrium

The beam axis, denoted  $x$ , is not necessarily a neutral axis. The axis corresponding to the direction of transverse displacements is denoted  $z$ , as shown in Fig. 1. For a Euler–Bernouli beam, the kinematical hypotheses are

$$\tilde{\mathbf{u}}(x, z) = \tilde{U}(x, z) \mathbf{e}_x + \tilde{W}(x, z) \mathbf{e}_z \quad \text{with} \quad \begin{cases} \tilde{U}(x, z) = \tilde{u}(x) - z \tilde{w}_{,x}(x), \\ \tilde{W}(x, z) = \tilde{w}(x). \end{cases} \tag{5}$$

The total axial displacement on the reference axis,  $\tilde{u}$ , and the transverse displacement,  $\tilde{w}$ , only depend upon  $x$ . In the remainder of this paper,  $x$  derivatives will be denoted by  $(\cdot)_{,x}$ . The kinematical assumption (5) implies that  $\tilde{E}_{xz} = 0$  (no shear strains). Besides, the assumption of plane stress yields

$$\tilde{S}_{yy} = \tilde{S}_{zz} = \tilde{S}_{xy} = \tilde{S}_{yz} = 0. \tag{6}$$

Assuming a linearly elastic isotropic material, we have

$$\tilde{S}_{xx} = E(\tilde{E}_{xx} - \alpha\theta_0), \tag{7}$$

$E$  and  $\alpha$  are, respectively, the Young’s modulus and the coefficient of thermal expansion. Then, under the assumption of small strain and large displacement, the terms  $\tilde{U}_{,x}^2$  and  $\tilde{U}_{,x}U_{i,x}$  are commonly regarded as higher-order effects, and thus neglected in Eq. (3) to finally give the following Von Karman axial strain:

$$\tilde{E}_{xx} = (\tilde{u} - z\tilde{w}_{,x})_{,x} + \frac{1}{2}\tilde{w}_{,x}^2 + w_{i,x}\tilde{w}_{,x}. \tag{8}$$

Now, it can be shown that the application of Hamilton’s principle of Section 2.1 yields the equilibrium equations:

$$\begin{cases} \tilde{N}_{,x} + \tilde{t}_x = \rho_m \ddot{\tilde{u}} - \rho_{mf} \ddot{\tilde{w}}_{,x}, \\ \tilde{Q}_{,x} + ((\tilde{w}_{,x} + w_{i,x})\tilde{N})_{,x} + \tilde{t}_z = \rho_m \ddot{\tilde{w}} \end{cases} \tag{9}$$

with the following natural or essential boundary conditions at  $x = 0, L$ :

$$\begin{cases} \tilde{N} = \int_A \tilde{T}_x dA \quad \text{or} \quad \tilde{u} = \tilde{u}, \\ \tilde{Q} + (\tilde{w}_{,x} + w_{i,x})\tilde{N} = \int_A \tilde{T}_z dA \quad \text{or} \quad \tilde{w} = \tilde{w} \quad \text{at } x = 0, L, \\ \tilde{M} = \int_A z\tilde{T}_x dA \quad \text{or} \quad -\tilde{w}_{,x} = \tilde{\beta} \end{cases} \tag{10}$$

$\tilde{N}$ ,  $\tilde{M}$ , and  $\tilde{Q}$ , respectively, denote the axial force, the moment and the transverse force resultants, given by

$$\begin{cases} \tilde{N} = \int_A \tilde{S}_{xx} dA = H_m \left( \tilde{u}_{,x} + \frac{1}{2}\tilde{w}_{,x}^2 + \tilde{w}_{,x}w_{i,x} \right) - H_{mf}\tilde{w}_{,xx} - N_T, \\ \tilde{M} = \int_A z\tilde{S}_{xx} dA = H_{mf} \left( \tilde{u}_{,x} + \frac{1}{2}\tilde{w}_{,x}^2 + \tilde{w}_{,x}w_{i,x} \right) - H_f\tilde{w}_{,xx} - M_T, \\ \tilde{Q} = \tilde{M}_{,x} + \tilde{m} - \rho_{mf}\ddot{\tilde{u}} + \rho_f\ddot{\tilde{w}}_{,x}. \end{cases} \tag{11}$$

The following notations have been used:

$$\begin{aligned} (H_m, H_{mf}, H_f) &= \int_A E(1, z, z^2) dA, (\rho_m, \rho_{mf}, \rho_f) = \int_A \rho_{\text{ref}}(1, z, z^2) dA, (N_T, M_T) = \int_A E\alpha\theta_0(1, z) dA, \\ \tilde{t}_x &= \int_A \rho_{\text{ref}}\tilde{f}_{,x} dA + \int_{\partial A} \tilde{T}_x ds, \tilde{t}_z = \int_A \rho_{\text{ref}}\tilde{f}_z dA + \int_{\partial A} \tilde{T}_z ds, \tilde{m} = \int_A \rho_{\text{ref}}\tilde{f}_x z dA + \int_{\partial A} \tilde{T}_{xz} ds. \end{aligned} \tag{12}$$

$A$  denotes the cross-sectional area in the reference configuration, and  $\partial A$  is its contour. The prestressed state verifies Eqs. (9)–(12) for the static case.

### 3.2. Prestressed dynamics (total Lagrangian formulation)

From Section 2.2, the total displacement components are decomposed as  $\tilde{u} = u_0 + u$  and  $\tilde{w} = w_0 + w$ . The expression of Table 1 for the total Lagrangian incremental strain yields the linearized incremental Green–Lagrange axial strain, which writes after neglecting terms  $U_{0,x}U_{,x}$  and  $U_{i,x}U_{,x}$ , of higher-order effects:

$$e_{xx} = (u - zw_{,x})_{,x} + w_{0,x}w_{,x}. \tag{13}$$

It can be verified that the above expression can also be obtained from a direct linearization of Eq. (8).

Now, we have

$$\mathbf{e} : \boldsymbol{\sigma} = e_{xx}\sigma_{xx} = E(e_{xx})^2; \quad \text{tr}(\nabla\mathbf{u}\boldsymbol{\sigma}_0\nabla\mathbf{u}^T) = u_{x,x}\sigma_{0,xx}u_{x,x} + w_{,x}\sigma_{0,xx}w_{,x}. \tag{14}$$

The first term of the right member of the second equality also involves terms of higher order effects and can be neglected (physically, this means that the effect of axial prestress is supposed negligible on the superimposed axial displacement). Using Eqs. (13) and (14) in (4), the following expressions of energies are finally obtained:

$$\left\{ \begin{array}{l} T = \frac{1}{2} \int_0^L \rho_m (\dot{u}^2 + \dot{w}^2) dx + \frac{1}{2} \int_0^L \rho_f \dot{w}_{,x}^2 dx - \int_0^L \dot{u} \rho_{mf} \dot{w}_{,x} dx, \\ V_{\text{ext}} = - \int_0^L u \bar{t}_x dx - \int_0^L w \bar{t}_z dx + \int_0^L w_{,x} \bar{m} dx - [u \int_A \bar{T}_x dA + w \int_A \bar{T}_z dA - w_{,x} \int_A z \bar{T}_x dA]_0^L, \\ V = \frac{1}{2} \int_0^L H_m u_{,x}^2 dx + \frac{1}{2} \int_0^L H_f w_{,xx}^2 dx - \int_0^L u_{,x} H_{mf} w_{,xx} dx + \frac{1}{2} \int_0^L N_0 w_{,x}^2 dx, \\ + \int_0^L u_{,x} H_m (w_{0,x} + w_{i,x}) w_{,x} dx - \int_0^L w_{,x} H_{mf} (w_{0,x} + w_{i,x}) w_{,xx} dx + \frac{1}{2} \int_0^L H_m (w_{0,x} + w_{i,x})^2 w_{,x}^2 dx. \end{array} \right. \quad (15)$$

The application of Hamilton's principle gives the equilibrium equations for prestressed dynamics. These equations are not shown here for conciseness, but it can be verified that they exactly correspond to a direct linearization of Eqs. (9)–(12).

The incremental strain energy  $V$  is dependent on two prestress variables: the “classical” axial preload  $N_0$ , and the predisplacement derivative  $w_{0,x} + w_{i,x}$ . Hence for dynamics, the predisplacement due to prebending is summed with that due to initial imperfections. The above expression of  $V$  shows that the presence of predisplacement induces some coupling between the axial and transverse superimposed displacements, and that its effect will be completely characterised by the product  $(w_{0,x} + w_{i,x})w_{,x}$ . This means that how a given mode will be affected by predisplacement will depend on how its own shape will be related to the shape of the predeformed geometry.

### 3.3. Numerical method

#### 3.3.1. FE interpolation

The above equations are solved using a FE method. In a conventional manner, a linear interpolation is chosen for the axial displacement  $u$  as well as the geometry. Hermitian interpolation functions are used for approximating the transverse displacement  $w$ . Then, on a reference element,  $u$  and  $w$  are discretized as follows:

$$u = \mathbf{N}_u^e \mathbf{u}^e; \quad w = \mathbf{N}_w^e \mathbf{w}^e \quad (16)$$

with

$$\begin{aligned} \mathbf{N}_u^e &= \left\langle \frac{1-\xi}{2}, \frac{1+\xi}{2} \right\rangle; \quad \mathbf{u}^{eT} = \langle u_1^e, u_2^e \rangle; \quad \mathbf{w}^{eT} = \langle w_1^e, -w_{1,x}^e, w_2^e, -w_{2,x}^e \rangle, \\ \mathbf{N}_w^e &= \left\langle \frac{1}{4}(1-\xi)^2(2+\xi), -\frac{L^e}{8}(1-\xi^2)(1-\xi), \frac{1}{4}(1+\xi)^2(2-\xi), -\frac{L^e}{8}(-1+\xi^2)(1+\xi) \right\rangle. \end{aligned} \quad (17)$$

$\xi$  is the reference coordinate varying from  $-1$  to  $+1$ . The subscripts  $i$  ( $i = 1, 2$ ) denote the local node number.  $L^e$  is the element length. Elements have three degrees of freedom per node associated to  $u$ ,  $w$ ,  $-w_{,x}$ . Obviously, the same choice of interpolating functions is made in the prestressed state analysis, for  $u_0$  and  $w_0$ .

#### 3.3.2. Prestressed state computation

The prestressed state is obtained by solving the static nonlinear system (9), denoted as  $\mathbf{K}_0 \mathbf{U}_0 = \mathbf{F}_0$  after FE discretization.  $\mathbf{K}_0 = \mathbf{K}_0(\mathbf{U}_0)$  is dependent on  $\mathbf{U}_0$ . However, this system may be efficiently solved with an iterative algorithm of Newton–Raphson type [38,39], by computing successive incremental displacement given by:  $\mathbf{R}(\mathbf{U}_0 + \delta \mathbf{U}) = 0$  where  $\mathbf{R} = \mathbf{F}_0 - \mathbf{K}_0 \mathbf{U}_0$  is the residue. A first-order Taylor expansion of  $\mathbf{R}$  leads to the following system:

$$\mathbf{K}_T^{j-1} \delta \mathbf{U} = \mathbf{R}^{j-1}, \quad (18)$$

where  $\mathbf{K}_T$  is the tangential stiffness matrix, defined by  $\mathbf{K}_T = \partial(\mathbf{K}_0 \mathbf{U}_0) / \partial \mathbf{U}_0 = \mathbf{K}_0 + \partial \mathbf{K}_0 / \partial \mathbf{U}_0$ . The superscript  $j-1$  denotes the step number in the iterative process and indicates that  $\mathbf{K}_T^{j-1}$  and  $\mathbf{R}^{j-1}$  are calculated from the solution  $\mathbf{U}_0^{j-1}$  of the previous step. The next step  $j$  is given by  $\mathbf{U}_0^j = \mathbf{U}_0^{j-1} + \delta \mathbf{U}$ .

### 3.3.3. Dynamics

After discretizing expressions (15) and assembling, the application of Hamilton’s principle yields the algebraic system:

$$\mathbf{M}\ddot{\mathbf{U}} + \mathbf{K}\mathbf{U} = \mathbf{F}, \tag{19}$$

where  $\mathbf{K}$  and  $\mathbf{M}$  are symmetric matrices.  $\mathbf{U}$  is the vector of unknown degrees of freedom.  $\mathbf{F}$  is the vector of external loads. In this paper, we will focus on eigenmodes, given by  $(\mathbf{K} - \omega^2\mathbf{M})\mathbf{U} = 0$ .

For clarity,  $\mathbf{K}$  is dependent on  $N_0$  and  $w_0 + w_i$  and may be decomposed as  $\mathbf{K}(N_0, w_0 + w_i) = \mathbf{K}_{\text{lin}} + \mathbf{K}_\sigma(N_0) + \mathbf{K}_L(w_0 + w_i)$ , defined as follows:

$$\begin{aligned} \frac{1}{2} \int_0^L H_m w_{,x}^2 dx + \frac{1}{2} \int_0^L H_f w_{,xx}^2 dx - \int_0^L u_{,x} H_{mf} w_{,xx} dx &= \frac{1}{2} \mathbf{U}^T \mathbf{K}_{\text{lin}} \mathbf{U}; & \frac{1}{2} \int_0^L N_0 w_{,x}^2 dx &= \frac{1}{2} \mathbf{U}^T \mathbf{K}_\sigma \mathbf{U}, \\ \int_0^L u_{,x} H_m (w_{0,x} + w_{i,x}) w_{,x} dx - \int_0^L w_{,x} H_{mf} (w_{0,x} + w_{i,x}) w_{,xx} dx + \frac{1}{2} \int_0^L H_m (w_{0,x} + w_{i,x})^2 w_{,x}^2 dx &= \frac{1}{2} \mathbf{U}^T \mathbf{K}_L \mathbf{U}. \end{aligned} \tag{20}$$

$\mathbf{K}_{\text{lin}}$  represents the small displacement stiffness matrix, usual in linear analysis.  $\mathbf{K}_\sigma$  is the geometric stiffness matrix, dependent on the axial prestress level.  $\mathbf{K}_L$  is a matrix due to the presence of predisplacement. The whole matrix  $\mathbf{K}$  may be not definite positive when buckling occurs but as stated earlier, we are interested in low prestressed states far from the buckling stage.

In fact, the above matrix  $\mathbf{K}$  may be directly obtained from the prestressed state computation because it exactly corresponds to the tangential stiffness matrix, previously defined. The procedure described in Section 3.3.2 is strictly equivalent to a linearization process around the step  $j-1$ , which means that  $\mathbf{K}_T^{j-1}$  is constructed in the same way as  $\mathbf{K} : \mathbf{K}_T^{j-1} = \mathbf{K}_{\text{lin}} + \mathbf{K}_\sigma(N_0^{j-1}) + \mathbf{K}_L(w_0^{j-1} + w_i)$ . In other terms, the stiffness matrix  $\mathbf{K}$  involved in (19) is equal to the tangential stiffness matrix  $\mathbf{K}_T^j$  of the final step  $j$ , when convergence is reached:  $\mathbf{K} = \mathbf{K}_T^j$ .

### 3.4. Note upon the updated Lagrangian formulation

In the presence of prebending, deriving the equilibrium equations from an updated Lagrangian formulation would require the theory of curved beams. For the sake of simplicity in this paper, the predeformed beam will be considered as a composition of straight beam elements (a proof of convergence when the number of elements tends to infinity can be found for the static case in Ref. [33]). Because we are interested in small prestrain states far from buckling situations, it is expected that relatively few elements will be required for a good convergence.

Let a straight beam element have a local axis  $x$ . This element is oriented in the global plane denoted  $(X, Z)$ . The local elementary degrees of freedom  $\mathbf{U}^e$  are related to the global ones through the transformation matrix  $\mathbf{T}^e$  defined by

$$\mathbf{U}^e = \mathbf{T}^e \mathbf{U}_g^e; \quad \mathbf{T}^e = \begin{bmatrix} \mathbf{q} & \mathbf{0} \\ \mathbf{0} & \mathbf{q} \end{bmatrix}; \quad \mathbf{q} = \begin{bmatrix} \cos \varphi & \sin \varphi & 0 \\ -\sin \varphi & \cos \varphi & 0 \\ 0 & 0 & -1 \end{bmatrix}; \quad \varphi = \widehat{X0x}. \tag{21}$$

No predisplacement terms appear in the updated Lagrangian formulation (see Table 1) because the predeformation is implicitly taken into account through the geometry meshed in its prestressed state. Hence, what has been presented in Section 3.3.3 can easily be extended to obtain the updated formulation, whose elementary matrices are now given by

$$\mathbf{M}_g^e = \mathbf{T}^{eT} \mathbf{M}^e \mathbf{T}^e; \quad \mathbf{K}_g^e = \mathbf{T}^{eT} (\mathbf{K}_{\text{lin}}^e + \mathbf{K}_\sigma^e) \mathbf{T}^e; \quad \mathbf{F}_g^e = \mathbf{T}^{eT} \mathbf{F}^e, \tag{22}$$

where  $\mathbf{M}^e$ ,  $\mathbf{K}_{\text{lin}}^e$ ,  $\mathbf{K}_\sigma^e$ , and  $\mathbf{F}^e$  have already been defined. The matrix  $\mathbf{K}_L^e$ , due to the presence of predisplacement in the total Lagrangian formulation, must not be taken into account in the updated stiffness matrix. The geometric stiffness matrix  $\mathbf{K}_\sigma^e$  remains because it corresponds to the effect of axial prestress, as shown in Eqs. (4). In the updated matrices defined by Eqs. (22), we have assumed that the changes in cross-section and density between the reference state and the predeformed state were negligible ( $dA_0 \simeq dA$  and  $\rho_0 \simeq \rho_{\text{ref}}$ ), which



is an acceptable approximation due to the small strain hypothesis. After assembling, the system to be solved is finally  $\mathbf{M}_g \ddot{\mathbf{U}}_g + \mathbf{K}_g \mathbf{U}_g = \mathbf{F}_g$ .

The updated Lagrangian formulation might yield some better convergence properties for general nonlinear analyses [33], may be computationally more effective [40] and simpler to implement in a FE code [34] because the terms in  $\mathbf{u}_0 + \mathbf{u}_i$  do not appear any more (the predeformation being implicitly included through the consideration of the predeformed geometry). Nevertheless in the present study, we are not interested in solving highly nonlinear problems and one advantage of the total Lagrangian formulation may be that the predeformation effects appear explicitly through terms in  $\mathbf{u}_0 + \mathbf{u}_i$ , which leads to somewhat more physical insight.

#### 4. A numerical example

A simple but illustrative example of a beam subjected to some significant thermal prebending is given. One considers a straight beam with neutral axis  $x$  ( $H_{mf} = \rho_{mf} = 0$ ) and constant properties  $H_m$ ,  $H_f$ ,  $\rho_m$ , and  $\rho_f$  along  $x$ . It is assumed that no initial imperfections are present ( $w_i = 0$ ). The horizontal beam is simply supported at both extremities: the transverse displacement and the moment are equal to zero at  $x = 0$  and  $L$ , as well as the axial displacement.

The static preload considered is a vertical thermal gradient along the beam thickness such that  $N_T = 0$  and  $M_T \neq 0$ , i.e. the thermal force and the thermal moment defined by Eqs. (12) are, respectively, zero and non-zero. For instance, such a case occurs with a temperature varying linearly from  $+\theta_0/2$  at the top ( $z = +h/2$ ) to  $-\theta_0/2$  at the bottom face ( $z = -h/2$ ) ( $E$  and  $\alpha$  being constant). From Eqs. (9) to (11), it can be seen that this choice of thermal load should mainly produce prebending because the axial prestress only results from the nonlinear coupling between the axial and transverse pre-displacements.

The beam has been discretized with 100 elements in order to ensure convergence (though less is needed). The numerical procedure is as follows. First, the static prestressed state is computed from the nonlinear model presented in Section 3.1 using the method in Section 3.3.2. Second, the eigenproblem of Section 3.3.3 is solved based on the computed prestressed state.

$x$  and  $\tilde{w}$  are, respectively, non-dimensionalized with respect to  $L$  and  $r$ , where  $r$  is the radius of gyration defined by  $r^2 = H_f/H_m$ . The resulting non-dimensional parameters of the problem can then be given by  $\max(w_0)/r$ ,  $N_0 L^2/H_f$ ,  $M_T L^2/rH_f$ . In this particular example, the beam predeflection greatly looks like a shape of  $\sin \pi x/L$  type ( $\max(w_0)/r$  is thus given by the predeflection at center) so that an approximate solution found by Kim et al. [16] may hold for the  $n$ th eigenfrequency:

$$\left(\frac{f_n}{f_{\text{ref}}}\right)^2 \simeq 1 + \frac{1}{n^2 \pi^2} \frac{N_0 L^2}{H_f} + \frac{1}{2} \left(\frac{w_0|_{L/2}}{r}\right)^2 \delta_{n1}, \quad (23)$$

where  $f_{\text{ref}}$  denotes the  $n$ th eigenfrequency without preload ( $M_T = 0$ ) and  $\delta$  is the Kronecker symbol.

Fig. 2 shows the non-dimensional axial prestress and vertical pre-displacement at center versus the thermal moment parameter  $M_T L^2/rH_f$  ranging from 0 to 6. The displacement remains less than 70% of the radius of gyration, which is small compared to the length  $L$  (less than 0.5%). This prestressed state is rather badly approximated by a linear state of small strain and small displacement (dashed line in Fig. 2). Although the difference in  $w_0$  is rather small between the linear and nonlinear theories (difference due to a stiffening effect, well-known in nonlinear mechanics), the nonlinear axial prestress  $N_0$  is not negligible for prestressed dynamics, as shown further. Note that if a linear theory is used, there is strictly no axial prestress.

Fig. 3 plots the change in the first eigenfrequency versus  $M_T L^2/rH_f$ . The eigenfrequency based on the complete nonlinear prestressed state (including  $N_0$  and  $w_0$ ) is compared with the same state but with  $w_0 = 0$ , arbitrarily neglected, in order to demonstrate the effect of prebending. It can be observed that the presence of prebending has a stiffening effect, significantly increasing the first eigenfrequency (+10% for  $M_T L^2/rH_f = 6$ ).

The eigenfrequencies based on a linear prestressed state ( $N_0 = 0$  in this example), also shown in Fig. 3, may lead to noticeable errors (2%). In the worst situation, the prestressed state would be computed with a linear theory (giving  $N_0 = 0$  here) and the eigenfrequencies would be computed without prebending, so that no



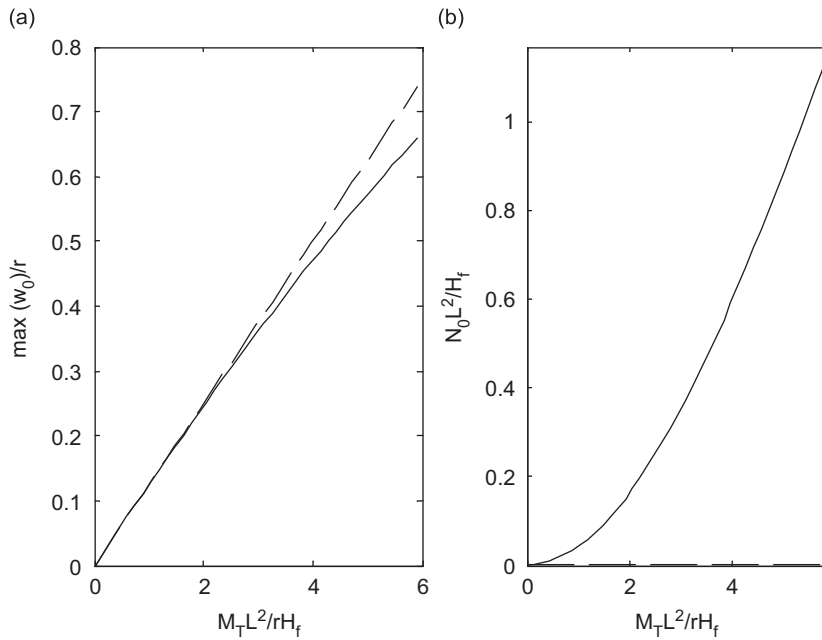


Fig. 2. (a) Non-dimensional predisplacement at center and (b) axial prestress versus thermal moment parameter. Solid lines: nonlinear computation, dashed lines: linear.

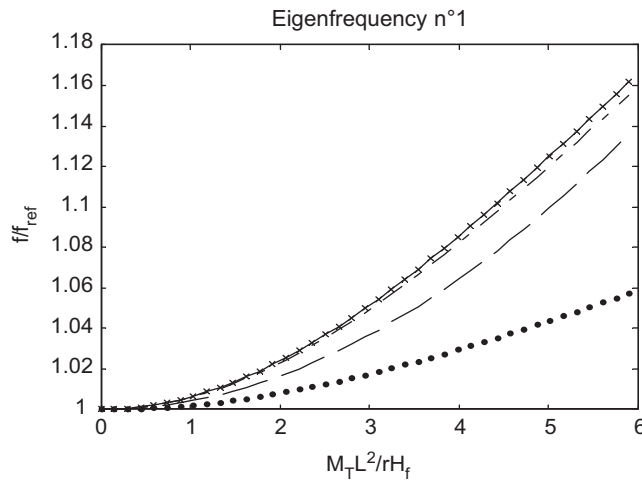


Fig. 3. First eigenfrequency ratio versus thermal moment parameter, obtained from a nonlinear prestressed state including (solid line) and neglecting (points) prebending, and from a linear prestressed state (dashed line). x-mark: results obtained from the updated formulation, dashed-dot line: analytical formula of Ref. [16].

change in eigenfrequencies could numerically be observed in that example. In that case, the error incurred on the first frequency would reach 16%.

The curve obtained with the updated formulation presented in Section 3.4 is also plotted on Fig. 3 (based on the complete nonlinear prestressed state). The meshed geometry corresponds now to the predeformed beam. Results exhibit a perfect agreement with the total Lagrangian formulation, which validates the prebending effects observed above. Besides, these results are in good agreement with the analytical results obtained from Eq. (23) (dashed-dot line in Fig. 3).

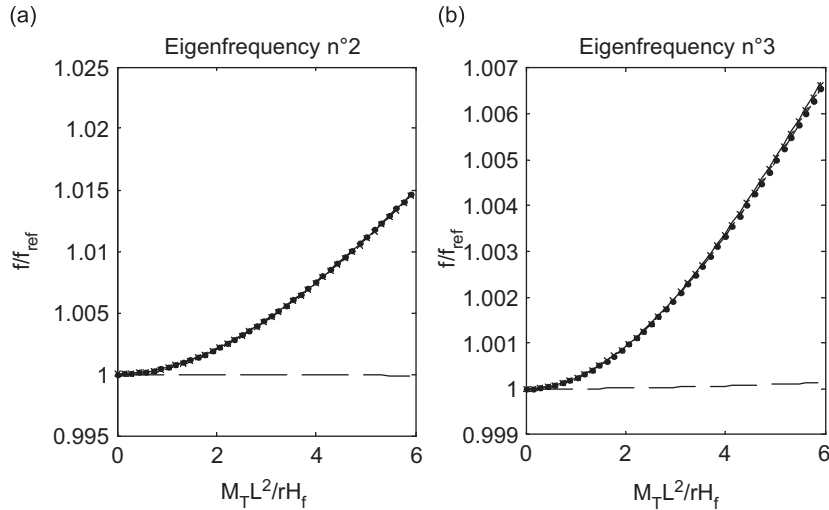


Fig. 4. (a) Second and (b) third eigenfrequencies ratios versus thermal moment parameter. The legend is the same as in Fig. 3.

The eigenfrequencies of modes 2 and 3 are given in Fig. 4. Neglecting nonlinearities of the prestressed state still leads to errors, smaller as the order of modes increases (1.5% and 0.7% for modes 2 and 3, respectively). However, prebending effects upon these modes are quite negligible. This insensitiveness to predisplacement is confirmed by the analytical formula (23) and was also observed in Refs. [18,19] when investigating the natural frequencies of simply supported buckled beams.

It must be outlined that modal shapes are not shown here for conciseness because they are standard for a simply supported beam (of  $\sin n\pi x/L$  type) and negligibly affected by prestress and prebending (at least, for the loading range considered here).

## 5. Experimental validation

In this section, a laboratory test-case for the study of flexural modes of a clamped planar beam thermally prestressed is presented. In a previous work [41], the experimental setup was satisfactorily tested on an axially prestressed straight beam, but with negligible predisplacement effects on modes. In this paper, a beam sensitive to the effect of prebending is considered. Experimental and FE eigenfrequencies are compared.

### 5.1. Experimental setup

The experimental device is depicted in Fig. 5. A vertical test beam is clamped at both ends on a workbench made of four vertical thick columns and two horizontal decks. This workbench is made of steel, whereas the beam is made of aluminum. The whole apparatus is set inside a climatic chamber with controlled ambient temperature.

Because steel and aluminum do not have the same coefficient of thermal expansion ( $1.17e-5$  and  $2.30e-5 \text{ K}^{-1}$ , respectively), a temperature change will naturally induce a significant axial prestress inside the beam. Because no external axial body force neither axial surface traction are present during the experiments (gravity effects are shown to be negligible), this quasi-static prestress  $N_0$  is constant along the beam—see Eq. (9)—even though a temperature gradient might exist along the beam.

One considers a beam of length  $L = 1 \text{ m}$  and  $0.03 \text{ m}$  depth (the length  $L$  is given without the additional ends,  $5 \text{ cm}$  each, used for clamping). As sketched in Fig. 5, the beam profile is circular on one face (straight on the other), so that no straight neutral axis exists ( $H_{mj} \neq 0$  and  $\rho_{mj} \neq 0$ ). The thickness varies from  $0.03 \text{ m}$  at extremities to  $0.01 \text{ m}$  at center. The cross-section is rectangular. The material properties are  $E = 7.24e + 10 \text{ Pa}$ ,  $\rho = 2790 \text{ kg m}^{-3}$ ,  $\alpha = 2.30e-5 \text{ K}^{-1}$  (aluminum 2017).

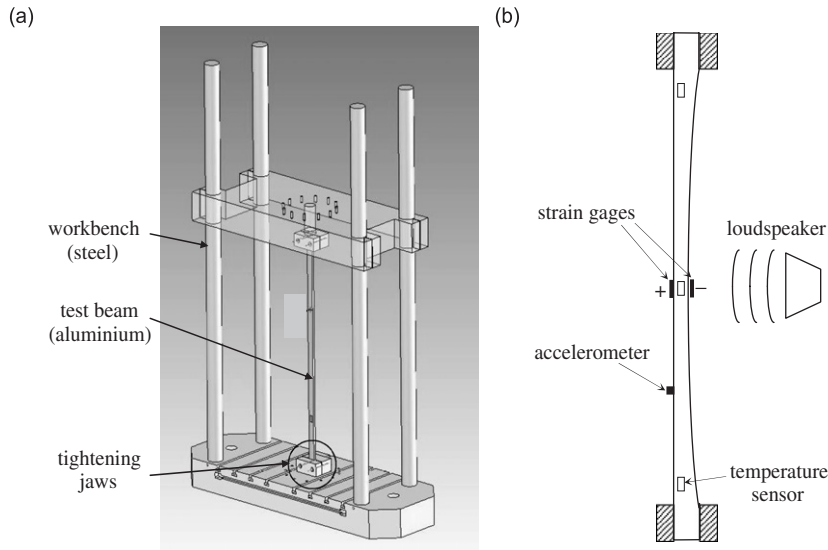


Fig. 5. (a) Workbench and (b) instrumented test beam.

Table 2  
Experimental and numerical free–free eigenfrequencies

Mode	Free–free		Clamped–free		
	Exp.	Num.	Exp.	Num.	Num. $C = 3e5$
1	40.3	39.9 (1.0%)	9.4	9.3 (1.1%)	9.3 (1.1%)
2	152.2	150.9 (0.9%)	72.1	73.1 (1.4%)	72.3 (0.3%)
3	341.3	342.3 (0.3%)	208.4	213.0 (2.2%)	209.2 (0.4%)

Clamped–free eigenfrequencies: experimental, numerical with a perfect clamping, and numerical with an adjusted torsional spring ( $C = 3e5 \text{ N m}$ ).

Those characteristics have been experimentally checked with some static bending tests (not shown for conciseness) and by comparing FE and experimental free–free eigenfrequencies, given in Table 2. The clamped–free frequencies have also been studied in order to characterise the experimental clamped boundary condition, imperfectly obtained with tightening jaws. This explains some slight differences between the experimental and numerical clamped–free eigenfrequencies (see Table 2). A torsional spring may be used in the model to approximate the real boundary condition as  $M = C(w,x)$ . A good match is found with a value of  $C = 3e5 \text{ N m}$ .

As depicted in Fig. 5, the test beam has been instrumented with one accelerometer, located at a node of the fourth flexural eigenmode in order to avoid nodes of modes 1–3. A pair of aluminum strain gages with thermal compensation has also been bonded to the beam center. Under the assumption of small strain, those gages provide a measure of the compensate strains  $\epsilon^{\pm} = E_{0xx}^{\pm} - \alpha^{\pm}\theta_0^{\pm}$  at the upper (+) and lower (–) sides. Some temperature sensors have helped checking that gage measurements were closely related to thermal variations.

It must be outlined that for the experiment, the uniformity of temperature on the cross-section of the beam can be assumed. In thermal engineering, the validity of this assumption may be evaluated by a Biot number less than 0.1:  $Bi = he/k < 0.1$  ( $h$ : heat exchange coefficient,  $e$ : beam thickness,  $k$ : thermal conductivity— $k = 134 \text{ W m}^{-1} \text{ K}^{-1}$ ). Though  $h$  is not known in the experiment, its value should be greater than  $450 \text{ W m}^{-2} \text{ K}^{-1}$  (with  $e = e_{\text{max}} = 0.03 \text{ m}$ ) in order to have  $Bi > 0.1$ , which exceeds with no doubt the actual value of  $h$ , given the weak convection inside the climatic chamber.

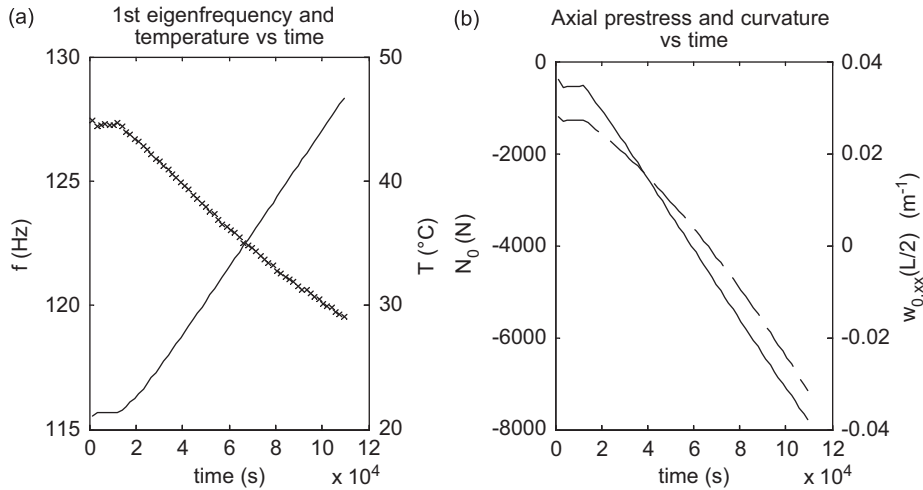


Fig. 6. Experimental results versus time: (a) averaged beam temperature (solid line) and 1st eigenfrequency ( $x$ -mark), (b) axial prestress (solid line) and center curvature (dashed line).

Then, under the assumption that the product  $\alpha\theta_0$  is constant on the cross-section, it can be shown that the curvature and the axial prestress are, respectively, obtained from the difference and the half-sum of strains:

$$w_{0,xx} = \frac{\varepsilon^- - \varepsilon^+}{e}; \quad N_0 = H_m \frac{\varepsilon^+ + \varepsilon^-}{2}, \quad (24)$$

where  $e$  is the beam thickness at the measuring point.  $N_0$  can thus be experimentally obtained without requiring any temperature sensor. Besides, only one measure at a given point is necessary, because it remains axially constant as stated earlier.

Tests are carried out inside the climatic chamber, first by stabilising the ambient temperature for 3 h, and then by heating for 27 h with a slope of  $+1^\circ\text{C}$  per hour. The beam is acoustically excited by a loudspeaker with a white noise input. Strain and temperature measurements are saved every one second. Acceleration measurements are automatically triggered every 30 min, for 250 s with a 1280 Hz sampling frequency, which is sufficient for the analysis of modes 1–3 (the eigenfrequency of the third mode is below 500 Hz).

Some experimental results are given in Fig. 6. They clearly show that the first eigenfrequency decreases as the average temperature increases versus time, whereas the axial prestress and the curvature decrease (note that the prestress is taken negative when compressive).

## 5.2. Results

### 5.2.1. Prestressed state

The knowledge of  $N_0$  and  $w_0(x) + w_i(x)$  is a crucial step. First, the initial imperfections  $w_i(x)$  must be measured. This has been done with an optical displacement sensor. The measured profile is depicted in Fig. 7. The initial imperfection between both ends is about 5.5 mm. Measurements have been fitted with a polynomial (of degree 3), as shown in Fig. 7, and then derived and interpolated on each node.

The computation of the prestressed state would a priori require the knowledge of the complete temperature field inside the beam, which is a problem beyond the scope of this paper. However, in the test-case considered, there is no prebending load (i.e. no load for the equilibrium equation governing the transverse displacement). In particular, the thermal moment  $M_T$  is zero because the temperature is cross-sectionally constant as stated earlier. This means that the knowledge of  $N_0$  is sufficient to determine the whole predeformed state, because the problem can be understood as a beam subjected to an axial preload enforced as a boundary condition at one extremity ( $x = L$  for instance).

Realistic boundary conditions should take into account the fact that (i) the clamped boundary condition is not perfect, (ii) tightening jaws are not perfectly perpendicular to the beam and make some angles with respect

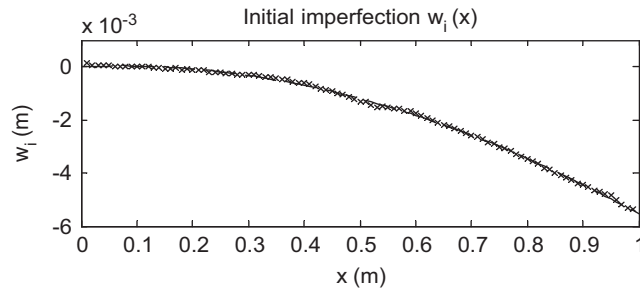


Fig. 7. Measured (x) and fitted (solid line) initial imperfections.

to the beam axis, denoted  $\bar{\beta}_1$  and  $\bar{\beta}_2$  at  $x = 0$  and  $L$ , respectively, and (iii) an additional displacement  $\bar{w}$  may be induced because of an alignment defect of the jaws. Finally, some adequate boundary conditions used for the prestressed state computation may be given by

$$\begin{cases} u_0 = w_0 = 0 & \text{and} & M_0 = -C(-w_{0,x} - w_{i,x} - \bar{\beta}_1) & \text{at } x = 0, \\ N_0 = \bar{N}, w_0 = \bar{w} & \text{and} & M_0 = -C(-w_{0,x} - w_{i,x} - \bar{\beta}_2) & \text{at } x = L. \end{cases} \quad (25)$$

$\bar{N}$  is the axial prestress measurement obtained from strain gages.  $\bar{w}$  is set to zero because the jaws position has been carefully adjusted to the imperfect beam in the experiment.  $C$  is the torsional stiffness already defined above. It should be noted that numerical tests have shown that a value of  $C = 3e5 \text{ N m}$  produces a negligible change of the prestressed state compared to a perfect clamping ( $C \rightarrow \infty$ ), but has been kept for a certain consistency with dynamics.

Now, the determination of  $\bar{\beta}_1$  and  $\bar{\beta}_2$  requires the measurement of the predeformed beam in its clamped–clamped configuration. This has been realised with the displacement sensor for two thermal states: one at the beginning, for  $N_0 = -0.40 \text{ kN}$  and  $w_{0,xx}(L/2) = +2.81e-2 \text{ m}^{-1}$ , and another nearly at the end of the test for  $N_0 = -7.66 \text{ kN}$  and  $w_{0,xx}(L/2) = -2.82e-2 \text{ m}^{-1}$ . The predeformed profiles are given in Fig. 8. Values of  $\bar{\beta}_1 = -0.5e-3 \text{ rad}$  and  $\bar{\beta}_1 = -1.5e-3 \text{ rad}$  were shown to give a good agreement of the FE model with the experimental data, as shown in Fig. 8. This agreement is further confirmed by Fig. 8, which also provides a comparison of the evolutions of experimental and FE curvatures at center throughout the test (evolutions being given with respect to the axial prestress instead of time).

### 5.2.2. Eigenfrequencies

In this test-case, the sensitivity of modal shapes with the prestressed states in the FE model was found to be quite negligible. Hence, we will exclusively focus on eigenfrequencies. For the computations, the following boundary conditions are applied:

$$u = w = 0 \quad \text{and} \quad M = -C(-w_{,x}) \quad \text{at } x = 0, L. \quad (26)$$

Some numerical tests have been realised in order to verify the influence of the torsional spring. Those tests demonstrate that there is no difference, with ( $C = 3e5 \text{ N m}$ ) or without ( $C \rightarrow \infty$ ) spring, in the relative change  $\Delta f/f_{\text{ref}}$  discussed later. The only effect of the spring in FE computations is a constant offset from the no spring case. This offset just enables a better match of numerical frequencies with the experiment, as already shown in Table 2.

Fig. 9 depicts the change in the first eigenfrequency with the axial prestress during the test. In the experiment, a decrease from 127.5 to 119.5 Hz is observed. The comparison between experimental and numerical results clearly demonstrates the stiffening influence of prebending: if only the axial prestress is considered in the computation of this eigenfrequency, a significant difference with experiment is found. If prebending is correctly included, the agreement becomes quite good. The relative change in frequency with respect to the reference frequency (corresponding to the beginning of the test) decreases to 6% at the end of the experiment, which is also found with the FE model based on a complete prestressed state. Without prebending, the numerical results give an erroneous change of about -11%.

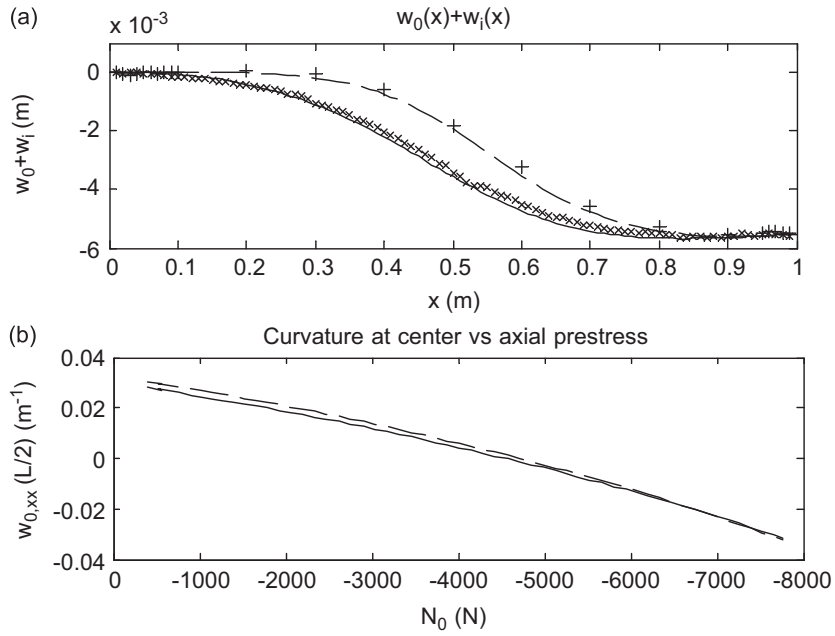


Fig. 8. (a) Predisplacement profiles of the clamped-clamped beam, measured (x) and computed (solid line) at the beginning of the experiment, measured (+) and computed (dashed line) at the end. (b) Experimental (solid line) and computed (dashed line) curvatures at center.

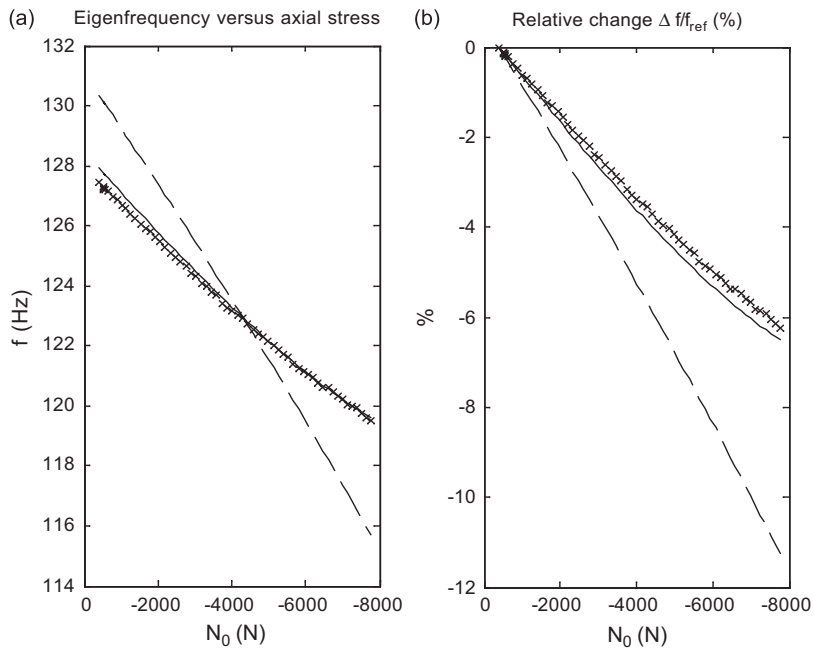


Fig. 9. (a) First eigenfrequency versus axial prestress: experimental (x), computed with prebending (solid line) and without (dashed line). (b) Relative change  $\Delta f/f_{ref}$  versus axial prestress (same legend).

The evolutions of eigenfrequencies of modes 2 and 3 are given in Fig. 10. The mode 2 (resp. 3) varies from 264.7 Hz (resp. 467.8 Hz) to 245.0 Hz (resp. 445.3 Hz), yielding a relative change of 7.3% (4.8%) at the end of the experiment. Even if prebending is neglected in the FE model, there is still a good agreement of numerical



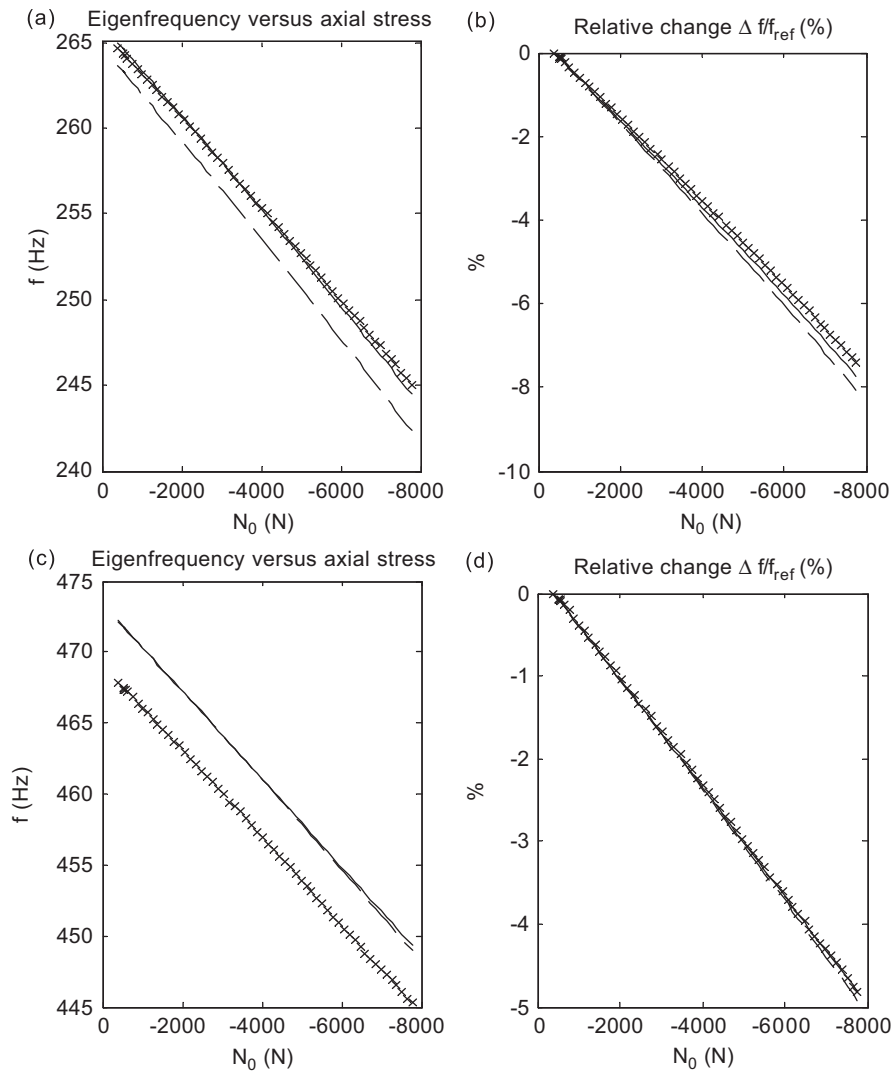


Fig. 10. (a) Second eigenfrequency and (b) its relative change versus axial prestress, (c) 3rd eigenfrequency, and (d) its relative change. The legend is the same as in Fig. 9.

results with the experimental relative change  $\Delta f/f_{ref}$ . This indicates that those modes are not very sensitive to prebending. A slight deviation can yet be observed for the eigenfrequency of mode 2 without prebending. For mode 3, the FE eigenfrequencies exhibit a small offset, less than 1%, due to the approximation of the boundary condition. But as far as the relative change is concerned, the agreement between the experiment and the model is satisfactory.

For the thermal loads considered in this experiment, the influence of predisplacement is thus only significant for the first mode. This is explained by the fact the sensitiveness to predisplacement of a given eigenfrequency depends on how its associated mode shape compares to the predeflection shape, combined with a stronger prestressing effect for lower eigenfrequencies. This phenomenon is coherent with results already observed, numerically or computationally, for vibrating buckled beams [16–19].

## 6. Conclusions

In the context of damage detection and structural health monitoring with thermal compensation, very small changes in modal parameters are sufficient to mask the presence of a disorder (or, inversely, to make a false

detection). This motivates the need of accurate models for prestressed dynamics. Based on a general theory, this paper proposes a numerical procedure that seems to be satisfying for beams. In the approach developed, the initial imperfections, prebending and geometrical nonlinearities of the prestressed state must all be included in the analysis, because they are shown to have a non-negligible impact upon eigenfrequencies. Those requirements are also likely to apply in the general framework of prestressed dynamics, concerning more complex structures such as frames or plates. This paper gives a background for further studies dealing with such structures.

From the numerical and experimental results above, when the beam predeformation is neglected, the axial prestress has a stronger shifting effect for lower eigenfrequencies. Nevertheless, this statement might not be true anymore in the presence of significant predisplacement, which tends to modify the shifting effects of axial prestress upon some isolated modes (the first one in the cases presented) due to a stiffening effect. In practice, neglecting predeflection and initial imperfections in eigenfrequency computations may lead to errors of several percents, even when the predisplacement remains relatively small compared to the beam length (always less than 0.5% in the examples of this paper).

### Acknowledgment

This research was partially supported by the project CONSTRUCTIF, in the framework of the French Computer and Security program (ACI S&I). The author wishes to thank engineers Jean-Pierre Desroche, Louis-Marie Cottineau and technician Jean-Philippe Gourdon in the Laboratoire Central des Ponts et Chaussées for their valuable technical assistance.

### References

- [1] A. Bokaian, Natural frequencies of beams under compressive axial loads, *Journal of Sound and Vibration* 126 (1988) 49–65.
- [2] J. Przybylski, L. Tomski, M. Golebiowska-Rozanow, Free vibration of an axially loaded prestressed planar frame, *Journal of Sound and Vibration* 189 (1996) 609–624.
- [3] D.J. Mead, Free vibrations of self-strained assemblies of beams, *Journal of Sound and Vibration* 249 (2002) 101–127.
- [4] S.S. Law, Z.R. Lu, Time domain responses of a prestressed beam and prestress identification, *Journal of Sound and Vibration* 288 (2005) 1011–1025.
- [5] M. Saiidi, B. Douglas, S. Feng, Prestress force effect on vibration frequency of concrete bridges, *Journal of Structural Engineering* 120 (1994) 2233–2241.
- [6] J.T. Kim, Y.S. Ryu, C.B. Yun, Vibration-based method to detect prestress-loss in beam-type bridges, *Proceedings of SPIE—The International Society for Optical Engineering*, 2003, pp. 263–274.
- [7] K.K. Raju, G.V. Rao, Free vibration behavior of prestressed beams, *Journal of Structural Engineering* 112 (1986) 433–437.
- [8] K. Sato, On the governing equations for vibration and stability of a Timoshenko beam: Hamilton's principle, *Journal of Sound and Vibration* 145 (1991) 338–340.
- [9] H. Abramovich, Natural frequencies of Timoshenko beams under compressive axial loads, *Journal of Sound and Vibration* 157 (1992) 183–189.
- [10] T. Yokoyama, Vibrations of a hanging Timoshenko beam under gravity, *Journal of Sound and Vibration* 141 (1990) 245–258.
- [11] S. Naguleswaran, Transverse vibration of a uniform Euler–Bernoulli beam under linearly varying axial force, *Journal of Sound and Vibration* 275 (2004) 47–57.
- [12] N. Ganesan, V. Pradeep, Buckling and vibration of sandwich beams with viscoelastic core under thermal environments, *Journal of Sound and Vibration* 286 (2005) 1067–1074.
- [13] H. Lurie, Lateral vibrations as related to structural stability, *Journal of Applied Mechanics* 19 (1952) 195–204.
- [14] R.L. Bisplinghoff, T.H.H. Pian, On the vibrations of thermally buckled bars and plates, *Ninth International Congress for Applied Mechanics*, Vol. 7, 1956, pp. 307–318.
- [15] S.M. Dickinson, The lateral vibration of slightly bent slender beams subject to prescribed axial end displacement, *Journal of Sound and Vibration* 68 (1980) 507–514.
- [16] C.S. Kim, S.M. Dickinson, The flexural vibration of slightly curved slender beams subject to prescribed axial end displacement, *Journal of Sound and Vibration* 104 (1986) 170–175.
- [17] N. Yamaki, A. Mori, Non-linear vibrations of a clamped beam with initial deflection and initial axial displacement, part I: theory, *Journal of Sound and Vibration* 71 (1980) 333–346.
- [18] N.C. Perkins, Planar vibration of an elastica arch: theory and experiment, *Journal of Vibration and Acoustics* 112 (1990) 374–379.
- [19] A.H. Nayfeh, W. Kreider, T.J. Anderson, Investigation of natural frequencies and mode shapes of buckled beams, *American Institute of Aeronautics and Astronautics Journal* 33 (1995) 1121–1126.
- [20] L.W. Chen, G.S. Shen, Vibration and buckling of initially stressed curved beams, *Journal of Sound and Vibration* 215 (1998) 511–526.

- [21] O. Paul, H. Baltes, Mechanical behavior and sound generation efficiency of prestressed, elastically clamped and thermomechanically driven thin film sandwiches, *Journal of Micromechanics and Microengineering* 9 (1999) 19–29.
- [22] S.R. Li, Z.C. Teng, Y.H. Zhou, Free vibration of heated Euler–Bernouli beams with thermal postbuckling deformations, *Journal of Thermal Stresses* 27 (2004) 843–856.
- [23] D. Addessi, W. Lacarbonara, A. Paolone, On the linear normal modes of planar pre-stressed curved beams, *Journal of Sound and Vibration* 284 (2005) 1075–1097.
- [24] J. Yang, S. Kitipornchai, K.M. Liew, Large amplitude vibration of thermo-electro-mechanically stressed FGM laminated plates, *Computer Methods in Applied Mechanics and Engineering* 192 (2003) 3861–3885.
- [25] S. Na, L. Librescu, H. Jung, Dynamics and active bending vibration control of turbomachinery rotating blades featuring temperature-dependent material properties, *Journal of Thermal Stresses* 27 (2004) 625–644.
- [26] M. Parisse, F. Curti, D. De Rosa, Dynamic response of a system driven by thermal actuation, *Advances in the Astronautical Sciences, Space Flight Mechanics 2004*, Vol. 119, 2005, pp. 821–832.
- [27] H. Sohn, M. Dzwonczyk, E.G. Straser, A.S. Kiremidjian, K.H. Law, T. Meng, An experimental study of temperature effects on modal parameters of the Alamosa canyon bridge, *Earthquake Engineering and Structural Dynamics* 28 (1999) 879–897.
- [28] B. Peeters, G. De Roeck, One year monitoring of the Z24 bridge: environmental effects versus damage events, *Earthquake Engineering and Structural Dynamics* 30 (2001) 149–171.
- [29] M. Basseville, F. Bourquin, L. Mevel, H. Nasser, F. Treysède, Handling the temperature effect in structural health monitoring: combining a subspace-based statistical test and a temperature-adjusted null space, *Third European Workshop on Structural Health Monitoring*, Granada, Spain, July 2006.
- [30] R.G. Rohrmann, M. Baessler, S. Said, W. Schmid, W.F. Ruecker, Structural causes of temperature affected modal data of civil structures obtained by long time monitoring, *Proceedings of the International Modal Analysis Conference (IMAC)*, San Antonio, USA, 2000, pp. 1–7.
- [31] K. Kanazawa, Structural damage detection from natural frequency eliminated by temperature effect, *Proceedings of the International Modal Analysis Conference (IMAC)*, St. Louis, USA, 2006.
- [32] E. Balmes, M. Corus, D. Siegert, Modeling thermal effects on bridge dynamic responses, *Proceedings of the International Modal Analysis Conference (IMAC)*, St. Louis, USA, 2006.
- [33] Y.-B. Yang, S.-R. Kuo, *Nonlinear Framed Structures*, Prentice-Hall, Singapore, 1994.
- [34] K.J. Bathe, *Finite Element Procedures*, Prentice-Hall, Englewood Cliffs, NJ, 1996.
- [35] Y.H. Pao, W. Sachse, H. Fukuoka, Acoustoelasticity and ultrasonic measurements of residual stresses, *Physical Acoustics*, Vol. XVII, Academic Press, Orlando, 1984, pp. 61–143.
- [36] C.Y. Chia, *Nonlinear Analysis of Plates*, McGraw-Hill, New York, 1980.
- [37] L. Librescu, W. Lin, Vibration of thermomechanically loaded flat and curved panels taking into account geometric imperfections and tangential edge restraints, *International Journal of Solids and Structures* 34 (1997) 2161–2181.
- [38] O.C. Zienkiewicz, R.L. Taylor, *The Finite Element Method—Vol. 2: Solid and Fluid Mechanics, Dynamics and Non-Linearity*, McGraw-Hill, London, 1998.
- [39] G. Dhatt, G. Touzot, *The Finite Element Displayed*, Wiley, London, 1984.
- [40] K.J. Bathe, S. Bolourchi, Large displacement analysis of three-dimensional beam structures, *International Journal for Numerical Methods in Engineering* 14 (1979) 961–986.
- [41] M. Basseville, F. Bourquin, L. Mevel, H. Nasser, F. Treysède, Merging sensor data from multiple temperature scenarii for vibration-based monitoring of civil structures, *Third European Workshop on Structural Health Monitoring*, Granada, Spain, July 2006.